Differential effects of oligosaccharides on the hydration of simple cations

Mats Eriksson,[1] Thisbe K. Lindhorst,[2] and Bernd Hartke[1,a)]
[1]*Institut für Physikalische Chemie, Christian-Albrechts-Universität, Olshausenstraße 40, 24098 Kiel, Germany*
[2]*Otto-Diels-Institut für Organische Chemie, Christian-Albrechts-Universität, Olshausenstraße 40, 24098 Kiel, Germany*

(Received 29 November 2007; accepted 24 January 2008; published online 12 March 2008)

Changed ion hydration properties near surfaces, proteins, and deoxyribose nucleic acid have been reported before in the literature. In the present work, we extend this work to carbohydrates: We have performed classical-mechanical molecular dynamics simulations to study solvation properties of simple cations of biological relevance (Na^+, K^+, Mg^{2+}, Ca^{2+}) in explicit water, near single and multiple oligosaccharides as glycocalyx models. We find that our oligosaccharides prefer direct contact with K^+ over Na^+, but that the Na^+ contacts are longer lived. These interactions also lead to strong but short-lived changes in oligosaccharide conformations, with oligosaccharides wrapping around K^+ with multiple contacts. These findings may have implications for current hypotheses on glycocalyx functions. © *2008 American Institute of Physics*. [DOI: 10.1063/1.2873147]

I. INTRODUCTION

Water is not the same everywhere in its liquid bulk phase. When the neighborhood of a water molecule changes from other water molecules to something else, one may expect that the local water structure, and hence, also the local solvation properties of water, will change accordingly. This expectation has been confirmed in recent decades, by experimental and theoretical studies of water structure and ion-solvation propensities in various situations, including, e.g., interfaces between the liquid water and air[1] as well as in confined situations[2] and clusters.[3,4]

Biological functions are often tied to well-defined interfaces and aqueous solutions often are one of the interacting partners. Hence, while bulk water properties clearly are very relevant for life, it is even more interesting to learn how interfacial water properties are modulated by biological systems to support biochemical functionality.

One of the most prominent, if not the most important biological interface in cell biology is the plasma membrane of cells which is found to be highly glycosylated in all cell types.[5] Eukaryotic cells are characterized by a typical "sweet"[6] surrounding, which is called the glycocalyx. This forms a nanodimensioned layer, consisting of a large number of structurally highly diverse glycoconjugates, which are partly embedded into the cell membrane with their noncarbohydrate moiety or stick to the cell surface by other noncovalent interactions.[7] This extremely complex macromolecular environment on cell surfaces cannot be characterized in all its molecular details owing to the inherent structural complexity and heterogeneity of cell surface carbohydrates.[8] Research in the field of glycobiology has revealed that the glycocalyx is essential for cellular communication,[9] however, the principles and mechanisms underlying its biological function are not well understood and are difficult to investigate.[10] The intermolecular interactions occurring on cell surfaces are of vital interest to better understand glycocalyx function. While carbohydrate-protein[11,12] and carbohydrate-carbohydrate interactions[13] have received a great deal of interest during the last years, investigation of carbohydrate-water as well as carbohydrate-water/ion interactions has been rather neglected until today.[14] As all participating molecules of the glycocalyx environment of eukaryotic cell surfaces are water exposed including the carbohydrate-recognition domains of lectins, the molecular interactions of carbohydrates in an aqueous, highly ionic system should receive great attention in glycobiology; even more so as most biological binding events occurring with carbohydrates have typically weak affinities.

Ion-specific effects in biological systems are directly related to the charge density and the resulting hydration properties of the ions. Using bulk water-water interaction energies as a reference, small monovalent ions are strongly hydrated and are classified as kosmotropes, whereas larger monovalent ions bind water weakly and are classified as chaotropes.[15] With this classification, Na^+ is a weak kosmotrope, or structure maker, in the sense that it has a relatively well defined and stable first hydration shell. The weak chaotrope K^+ is more flexible in its coordination with water and has a less stable and more dynamic first hydration shell as water-water interaction dominates over ion-water interactions. These simple differences in the balance between the interactions water-water, Na^+-water, and K^+-water have already been used successfully by one of the present authors[16] for a simple but effective explanation of the strikingly different structural propensities in cation-water clusters of Na^+ and K^+.

The differences in hydration properties between Na^+ and K^+ also are projected onto their interaction with biomolecules. Studies of potassium channels have shown that the free energy barrier for replacing K^+-coordinated water molecules by the carbonyl oxygen atoms of proteins in the inte-

a)Electronic mail: hartke@phc.uni-kiel.de.

rior of the channel is small compared to that of Na^+ and allows for a quick and selective transportation of K^+.[17] Carillo-Tripp *et al.*[18] showed that the cost of constraining a hydrated potassium ion inside a narrow nanopore is lower than that of constraining a sodium ion and that this is a result of the higher geometrical flexibility of potassium ions in their coordination with water. The simulation studies of Chen *et al.*[19] found a higher binding preference of Na^+ to the phosphate groups of deoxyribose nucleic acid (DNA) and a higher density of K^+ ions near the polar groups in the grooves of the DNA. A recent investigation of Na^+/K^+ affinities to different proteins by Vrbka *et al.*[20] observed a strong preference of Na^+ over K^+ close to the surface of different proteins, where the ion selectivity stems from cation specific interactions with sidechain carboxylate groups.

In this study, we have investigated the static and dynamic behavior of sodium and potassium around a third group of important biomolecules, the cell surface carbohydrates of the glycocalyx. Though the glycoconjugate pattern occurring on cell surfaces is cell-type specific, as well as characteristic for the developmental stage of the cell, a series of glycan structure types is common to most eukaryotic cell surface environments and grouped according to certain features. Among the group of glycoproteins, the so-called *N*-glycoproteins carry the *N*-glycans bound to the sidechain of an asparagine amino acid of the protein moiety via an *N*-glycosidic linkage to *N*-acetylglucosamine, which forms the nonreducing end in all *N*-glycans. All *N*-glycoproteins share a particular internal pentasaccharidic region, which is called the "core region." It consists of a branched structure Man(α1,6)[Man(α1,3)]Man(β1,4)GlcNAc(β1,4)GlcNAc, with the terminal GlcNAc *N*-glycosidically linked to an asparagine residue of the peptide chain in β mode. Branching out from this uniform core are oligosaccharide chains of diverse structural variety achieved by the attachment of different saccharides, leading to multiple branched structures, which have been classified into three types, those of the "high-mannose" type, the "complex" type and the "hybrid" type. Oligosaccharide moieties in glycoconjugates typically consist of up to 20 monomers, but they may also be much larger or smaller. For our modeling studies we selected an octasaccharidic branched *N*-glycan of the high-mannose type, which is depicted in Fig. 1 and can be abbreviated as $Man_6GlcNAc_2$. In addition to the typical core pentasaccharide it contains three α-mannosyl residues as (1,2), (1,3), and (1,6) branches.

Solvation properties of isolated, single carbohydrate units or short oligomers in water have been studied experimentally[21] and theoretically.[22–24] To our knowledge, however, neither hydration properties of larger oligomeric saccharides, nor differential solvation effects of such carbohydrates on cations, nor possible collective effects of several (oligomeric) saccharide units have been simulated before.

The remainder of this paper is organized as follows: In Sec. II we briefly summarize the most important technical details of our molecular dynamics (MD) calculations. Section III first contains some considerations on the validity of the force field descriptions used, followed by a presentation and discussion of several aspects of ion solvation in the neighborhood of our model saccharide. The findings are briefly summarized in the final Sec. IV.

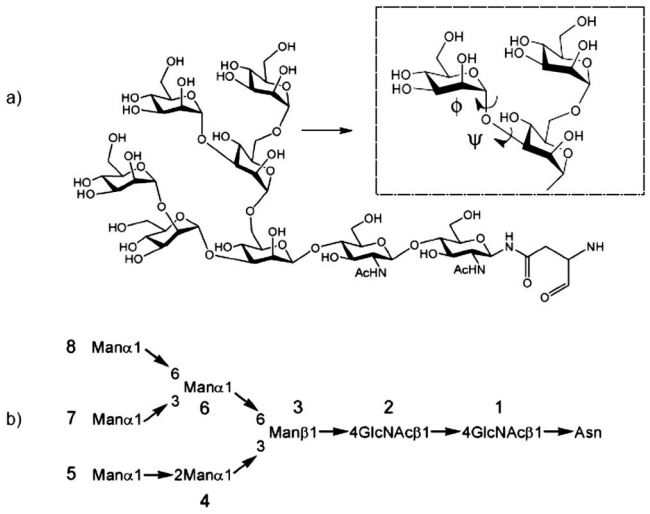

FIG. 1. Structure of the branched asparagine-linked *N*-glycan $Man_6GlcNAc_2$ used for modeling studies: (a) in detail, together with a zoomed-in part showing the two dihedral angles ϕ and ψ describing the Man(7)(α1−3)Man(6) glycosidic linkage and (b) in its abbreviated form with used numbering of monosaccharide residues [(1)–(8)] indicated.

II. METHODS

The basic oligosaccharide unit $Man_6GlcNAc_2$ used in all our calculations is shown in Fig. 1. Classical-mechanical MD simulations were carried out on systems consisting either of one isolated $Man_6GlcNAc_2$ unit or of an array of nine of these units, in either 0.15 M NaCl or 0.15 M KCl aqueous solution. The single oligosaccharide/ion systems were all set up the same way. The saccharide was solvated in a large water box with unit cell dimensions of 51.88 Å × 72.31 Å × 48.93 Å. This setup models an isolated saccharide, separated from its periodic images by approximately 50 Å, on an imaginary surface spanned by the *xz* plane of the simulation box. Na^+, K^+, Mg^{2+} or Ca^{2+} and Cl^- ions were randomly added to the box by removing overlapping water molecules. The resulting NaCl and KCl systems consisted of 6132 water molecules, 17 sodium or potassium ions, and 17 chloride ions. Systems of higher carbohydrate density were set up in a similar way. Nine *N*-linked $Man_6GlcNAc_2$ oligosaccharides were placed in a regular arrangement in the simulation box, each saccharide separated by approximately 20 Å (see Fig. 2). This setup models a dense saccharide array located on the imaginary surface spanned by the *xz* plane of the simulation box. A large *y* dimension of the box was chosen to model a bulk water environment above the saccharide array, giving box dimensions of 74 Å × 80 Å × 74 Å. For these systems, 34 sodium or potassium ions were added together with 34 chloride ions, giving a final number of 12 718 water molecules. Starting conformations of the saccharides were taken from the SWEET database.[25]

All ion force fields used in this study treat the ions as simple point-charged, nonpolarizable Lennard-Jones particles. Na^+, K^+, and Cl^- force fields are from Beglov and

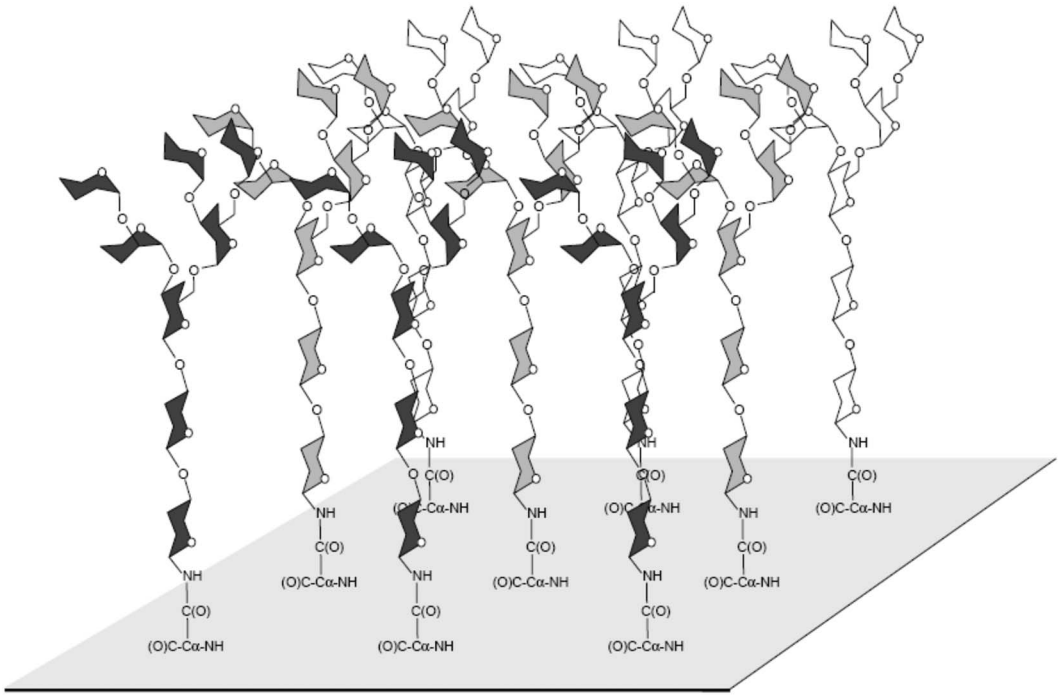

FIG. 2. Graphical display of the array of *N*-linked $Man_6GlcNAc_2$ oligosaccharides.

Roux.[26] Lennard-Jones parameters for Mg^{2+} and Ca^{2+} were calculated using the Aaqvist parameters[27] together with TIP3P water, giving (r, ϵ) values of (1.5734 Å, 0.87504 kcal/mol) and (2.6522 Å, 0.44966 kcal/mol) for Mg^{2+} and Ca^{2+}, respectively. Both the carbohydrate force field, GLYCAM04,[28] and ion parameters used in this study, were developed together with the TIP3P water model,[29] giving a consistent set of parameters for the whole system.

All systems were simulated using NAMD version 2.6,[30] using the same simulation protocol/parameters. Minimization, heating to 300 K at constant volume, and equilibriation at a constant pressure of 1 bar was followed by production runs in the NVT-ensemble, using a 2 fs integration time step, for a total of 60 ns. The temperature was controlled by the Berendsen thermostat[31] with a time constant of 5 ps. Long range electrostatic interactions were accounted for using PME.[32] Lennard-Jones interaction was cutoff at a distance of 12 Å, without using switching functions. SHAKE[33] was used to constrain all heavy-atom-hydrogen bonds. Positional restraints were applied to the main-chain asparagine atoms in the *N*-link [C_α, N, and C(O)], allowing no diffusional motion of the saccharides and restraining each saccharide to the *xy* plane of the simulation box. 1–4 bonded electrostatic and van der Waals scaling was set to unity in accordance with the GLYCAM04 force field.[34] Coordinates were saved every 0.4 ps of the trajectories, giving 150 000 frames for data analysis. All results presented in this paper were calculated with the ptraj module of the AMBER molecular dynamics package,[35] which we extended and modified to allow for a better analysis of our highly flexible oligosaccharides, as partly described in the following:

Distribution of the cations around the saccharides are investigated using proximal distribution functions calculated as

$$g_{\mathrm{prox},i}(r) = \frac{\langle n_i(r,\Delta r)\rangle}{\rho_i \langle V_s(r,\Delta r)\rangle}. \tag{1}$$

Here $\langle n_i(r,\Delta r)\rangle$ is the average number of ions within a shell of thickness Δr at distance r from the closest saccharide atom. ρ_i is the bulk density of the ion, and $\langle V_s(r,\Delta r)\rangle$ is the average volume of the shell. The volume of each shell depends on the conformation of the saccharide and is calculated as an average over the trajectory, as proposed by Ashbaugh *et al.*[36] The instantaneous volume of the shell at distance r and thickness Δr is calculated from the surface area of the union of spheres with radii r, centered on each saccharide atom j,

$$V_s(r,\Delta r) = \sum_j \Omega_j(r) r^2 \Delta r, \tag{2}$$

where $\Omega_j(r)r^2$, $0 \le \Omega_j(r) \le 4\pi$, is the accessible surface area of the sphere of radius r centered at atom j, determined by a Monte Carlo sampling. Ion-water or ion-ion distributions are calculated by standard radial distribution functions. In this case, the volume in Eq. (1) is static, and simply calculated as $4\pi r^2 \Delta r$.

Residence times of saccharide bound ions, or water molecules in the first hydration shell of the ions, are calculated from the "layer survival-time-correlation function" $C_R(t)$,[37,38] defined as

$$C_R(t) = \frac{1}{N_J} \sum_{j=1}^{N_J} \frac{\langle p_{R,j}(0) p_{R,j}(t)\rangle}{\langle p_{R,j}(0)\rangle^2}. \tag{3}$$

$p_{R,j}(t)$ is a binary function associated with each atom, ion, or molecule j under investigation and is unity whenever species j was in the layer at a given time origin and remains in the layer R for the time period t, without leaving the layer at any

intermediate time step, and zero otherwise. Average residence times can be calculated directly from $C_R(t)$, which gives the probability that, for instance, a water molecule remains in a given volume around an ion for a time period t.

The conformational dynamics of the saccharides is investigated by dihedral autocorrelation functions calculated as[39]

$$C_A(t) = \langle \cos(\theta(\tau) - \theta(\tau + t)) \rangle. \quad (4)$$

$C_A(t)$ shows to which degree the dihedral angle θ at time τ correlates with that at the later time $\tau+t$. The glycosidic dihedral angles ϕ and ψ are defined as H1-C1-OX-CX and C1-OX-CX-HX for a $(1 \rightarrow X)$ $(X=2,3,4)$ linkage, analogous to the ϕ_h and ψ_h definition in the IUPAC convention.[40]

To test the statistics of our collected data, the simulation times for the single saccharide (NaCl/KCl) simulations were extended to 90 ns. Only minor differences could be seen in distributions and observed saccharide coordination numbers for these longer simulations, indicating that the results presented in this study are based on sufficient sampling.

Some further technical details will be mentioned at appropriate places throughout the presentation of the results, to make their presentation easier for the reader.

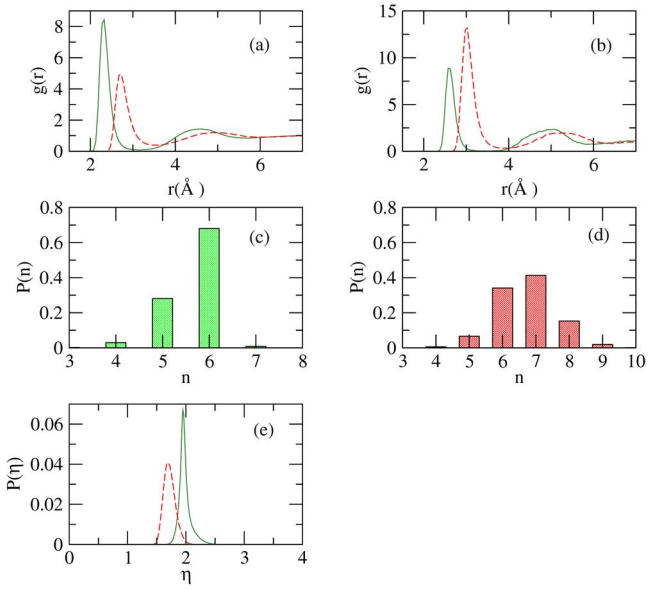

FIG. 3. (Color online) Various hydration properties of Na^+ and K^+: (a) Na^+ (solid line) and K^+ (dashed line) water oxygen radial distribution functions. (b) Na^+ (solid line) and K^+ (dashed line) Cl^- radial distribution functions. Distributions of instantaneous cation-water oxygen coordination numbers for Na^+ (c) and K^+ (d). (e) Probability distributions of asphericity parameters of cation Voronoi polyhedra for Na^+ (solid line) and K^+ (dashed line).

III. RESULTS

A. Ion hydration and force fields

Recent studies have shown that the structuring or destructuring effects of monovalent ions on hydration water is limited to water molecules in direct contact with the ion, i.e., first hydration shell water molecules.[41,42] These studies show the importance of local structural and dynamical properties of ion-water interactions for describing hydration phenomena and resulting ion-specific effects observed in biological systems. Hence, we begin by presenting various structural and dynamical properties of the cation-first hydration shell complex for the two most important ions for this study, Na^+ and K^+, calculated from the carbohydrate/ion/water trajectories (see Sec. II) in volumes of the simulation box where water has bulk properties. Given the obvious limitations of studying ion hydration with standard force fields, it is interesting to see how these force fields can distinguish between the kosmotropic/chaotropic character of the two cations and to which degree calculated hydration properties agree with experiment and with simulations at higher levels of theory.

The structure of the first hydration shell around the cations is more or less flexible and can take different conformations. In a first approximation, it can be quantified by the coordination number, i.e., the average number of water molecules in direct contact with the cations. The coordination numbers of Na^+ and K^+ can be calculated by integrating the cation-water oxygen radial distribution functions (RDFs) from zero up to the first minimum, cf. Fig. 3(a). They are found to be 5.7 and 6.7 for Na^+ and K^+, respectively. A more detailed picture of the hydration structure around the two cations is provided by the probability distributions of the instantaneous coordination numbers, shown in Figs. 3(c) and 3(d). The first hydration shell of K^+ is clearly much more flexible than that of Na^+, allowing for a wider range of possible conformations. Na^+, on the other hand, can be seen to be rather restrictive in its coordination with water, which takes place almost exclusively through five- or sixfold coordination.

The geometry of the cations and their coordinated water is investigated from properties of Voronoi polyhedra[43] constructed around the ions. The asphericity parameter[44] describes the shape of the ion Voronoi polyhedra. It is unity for a sphere, and takes values of 1.21, 1.32, 1.65, 1.91, and 3.31 for an icosahedron, a dodecahedron, an octahedraon, a cube, and a tetrahedron, respectively. The distribution plots of the asphericity parameters for Na^+ and K^+ in Fig. 3(e) show a narrow distribution around a close to cubic shape of the Na^+ Voronoi polyhedra, thus indicating an on average close-to-octahedral shape of Na^+ together with the on average close to six coordinated water molecules. Larger deviations can be seen for K^+ from any standard coordination polyhedron.

Coordination numbers provide an important link between experiment and simulations. However, difficulties involved in extracting radial distribution functions and coordination numbers from scattering data have resulted in measured coordination numbers in the range of 4–8 for both Na^+ and K^+.[45] An alternative source for structural ion hydration data for force field validation is simulations using *ab initio* approaches.[45–47] Compared to the calculated coordination numbers from these studies, which are in the range 4.3–5.2 for Na^+ and 5.8–7.0 for K^+, the force fields used in this study tend to overestimate the coordination numbers. Nevertheless, given the uncertainty in experimental and computational coordination numbers, they can be considered to provide a reasonable model for the hydration structures of both cations.

Calculated self-diffusion coefficients for Na^+ and K^+ and average residence times of water in the first hydration shell

TABLE I. Ion-water solvation data from our MD simulations.

	r (Å) [a]	ϵ (kcal/mol) [a]	n_{coord} [b]	D (10^{-5} cm^2/s) [c]	τ_{res} (ps) [d]
Na^+	2.7275	0.0469	5.7	1.43	19.5
K^+	3.5375	0.0870	6.7	2.28	4.1

[a]Ionic van der Waals parameters, from Beglov and Roux (Ref. 26).
[b]Cation-water coordination numbers, calculated from the radial distribution functions in Fig. 3(a).
[c]Diffusion coefficients, calculated from the average mean square displacement of respective cation.
[d]Average residence times [see Eq. (3)] for water molecules in the first hydration shell of the cations, defined by a spherical volume with a radius corresponding to the distance of the first minima of the cation-water RDFs in Fig. 3(a).

of respective cation are presented in Table I. The dynamics of the cations and the hydration water reflect the fundamental difference in hydration properties of Na^+ and K^+. The chaotropic nature of K^+ is reflected in shorter residence times of hydration water and a higher overall mobility. The hydration shell of the weak kosmotrope Na^+ is by comparison relatively rigid and lowers the mobility of Na^+. Compared to the experimental diffusion coefficients at infinite dilution, 1.334 and 1.957×10^{-5} cm^2/s for Na^+ and K^+, respectively,[48] the mobilities of both cations are overestimated. However, this is likely due to the overly diffusive TIP3P water model[49] rather than an indication of problems with the ion force fields. The calculated residence times for first shell hydration water around both cations are overestimated, compared to experimental values,[50] but are in reasonable agreement with other simulation studies using different force fields.[42,51]

At higher ion concentrations, needed for a statistical analysis of ion distributions around biomolecules, a proper description of cation-anion interaction becomes important. Experimental data on these interactions is lacking, but simulations using standard force fields and *ab initio* approaches both show that Na^+ and K^+ form inner sphere contacts with Cl^- in solution, but the extent to which this occurs is greatly overestimated for certain force fields.[52] The cation-anion RDFs in Fig. 3(b) show a similar but slightly higher tendency of K^+ to pair with Cl^- over Na^+ in solution. The height of the first peaks are comparable to those found in the first principle simulations of Cavallari *et al.*[47] Reference simulations were also performed with ion parameters from the AMBER ff99 (Ref. 53) force field. These simulations showed a much higher tendency for ion-pairing in general, and in particular ion-pairing was enhanced approximately fivefold for K^+. For a comparative analysis of ion affinities, such large differences in cation-anion pairing tendencies will be projected onto the results, making these parameters unsuitable for our purposes.

B. Single saccharide-ion interaction

The results presented here are calculated from molecular dynamics simulations of one single $Man_6GlcNAc_2-Asn$ unit (cf. Fig. 1), in 0.15 M NaCl or KCl solution.

The distributions of Na^+ and K^+ around the oligosaccharide are shown in Fig. 4(a). The distribution functions are calculated with respect to the closest nonhydrogen atom of the saccharide and normalized with respect to the bulk density of the ions [cf. Eq. (1)]. Both distribution functions show a distinct first peak located at a distance equivalent to the first peak of the cation-water distributions [see Fig. 3(a)]. Here, this peak represents the case where one or more ion-coordinated water molecules have been replaced by contacts with the polar oxygens (or the 2-nitrogen atom of the *N*-acetyl-D-glucosamine residues) of the saccharide. A second broader peak is also visible for both cations which correspond to water mediated saccharide interactions. The different radial positions of these two peaks for Na^+ and K^+ simply reflect the different sizes of these ions. However, the differing relative heights of the first to the second peak indicate a different behavior of Na^+ and K^+ as they approach the saccharide: Apparently, K^+ has a greater probability of forming direct contacts with the saccharide, while Na^+ has a higher probability of forming water-separated saccharide contacts.

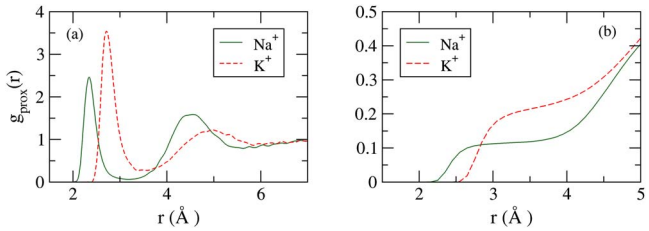

FIG. 4. (Color online) (a) Normalized $Man_6GlcNAc_2$-cation proximal distribution functions, calculated with respect to the closest nonhydrogen atom in the saccharide. (b) The corresponding cumulative sums (integrated distribution functions).

The result of this difference in the ion distributions can be further interpreted with the cumulative sums of Fig. 4(b). These cumulative sums show the average numbers of ions per frame, within a given distance of the saccharide. Again, the different radial "onset" of the two curves merely reflects the different ion sizes. More interesting is the difference in the height of the first step. Since the different volumes of the two ions have been taken into account (see earlier), the data for the two ions are directly comparable. Hence, it is clear that on average there are approximately twice as many potassium ions in direct contact with the saccharide. This result could be expected from the difference in hydration strength of the two ions. There will obviously be a higher energetic barrier in the case of Na^+ to remove a coordinated water and replace it with a saccharide contact. However, hydration properties of the ions alone cannot explain ion affinities to biomolecules. As mentioned in Sec. I, ion affinities vary between different bioligands (proteins, lipids, carbohydrates), and also vary with, e.g., the electrostatic character of the ion binding sites and their steric propensities.

Based on purely enthalpic arguments, Collins[54] recently proposed the so called law of matching water affinities, which states that the degree to which oppositely charged ions form ion-pairs in solution is determined by the difference in hydration energies between the cation and anion. Forming inner sphere contacts between two ions is only energetically favorable when the cost of removing coordinated water molecules is compensated by the newly formed cation-anion and water-water interactions. Within this theory, the formation of

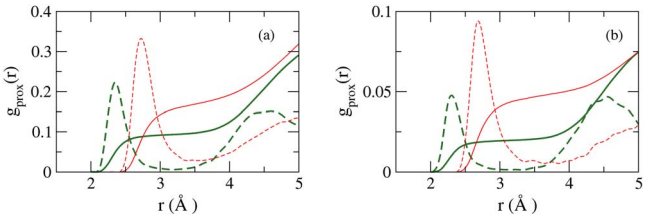

FIG. 5. (Color online) Proximal distribution functions (dashed lines) and cumulative sums (solid lines) for Na^+ (thick lines) and K^+ around $Man_6GlcNAc_2$ hydroxyl oxygen atoms (a) and endocyclic and glycosidic oxygen atoms (b). The distribution functions are multiplied by a constant factor for a clearer representation.

kosmotrope cation and anion pairs is driven by the energetic gain from cation-anion interactions, whereas chaotropic cation and anion pairing is driven by the energetic gain from water-water interactions formed by released water molecules.[15] For the relatively strongly hydrated biologically common phosphate and carboxylate anions, the law of matching water affinities predicts a greater affinity for Na^+ over K^+, which is supported by the studies of Vrbka *et al.*[20] and Cheng *et al.*[19] Similar arguments can be applied to the polar oxygen and nitrogen atoms of uncharged carbohydrate moieties, which can be considered to be weakly hydrated anions of low charge density, and would have a greater tendency of pairing with K^+. This trend can also be seen in ion affinities to the two different types of oxygen atoms of the saccharide. Figure 5 shows the proximal distributions and cumulative sums around the hydroxyl oxygens and the glycosidic and endocyclic oxygens of the saccharide. The relative difference in ion affinities is indeed larger around the lower charge density glycosidic and endocyclic oxygens.

Simulations were also performed with the divalent cations Ca^{2+} and Mg^{2+}; the corresponding distribution plots are shown in Fig. 6. The average cation-water oxygen distance calculated from the RDFs (not shown here) is approximately 2 and 2.4 Å for Mg^{2+} and Ca^{2+}, respectively. Figure 6 does not show a single inner sphere contact between the saccharide and Mg^{2+} in the whole 60 ns simulation and only a very small number of direct saccharide-Ca^{2+} contacts. However, the distributions of both cations show distinct peaks at distances corresponding to water separated contacts. This shows a clear correlation between the charge density and the behavior of the cations as they approach the saccharide surface. The tendency of the cations to form direct, inner sphere con-

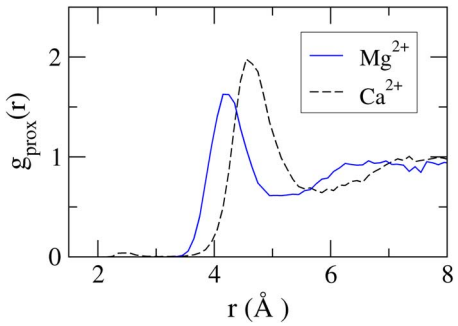

FIG. 6. (Color online) Normalized proximal distribution functions for Mg^{2+} (solid line) and Ca^{2+} (dashed line), calculated with respect to the closest nonhydrogen atom in $Man_6GlcNAc_2$.

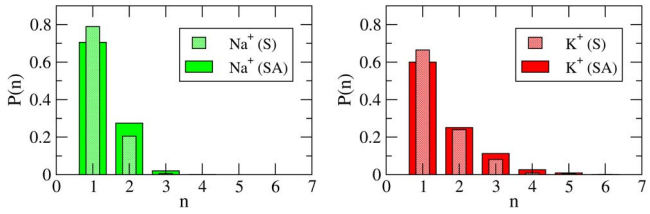

FIG. 7. (Color online) Probability distributions of cation-saccharide coordination numbers for Na^+ (left) and K^+ (right) bound to $Man_6GlcNAc_2$ (S) or to the array of $Man_6GlcNAc_2$ saccharides (SA).

tacts with the saccharide decreases with increasing charge density and stronger hydration in the series $K^+ > Na^+ > Ca^{2+} > Mg^{2+}$. For the divalent cations, these results indicate that interactions with polar noncharged saccharides almost exclusively take place through water-mediated contacts. Again, the observed ion affinities can be seen to change with the electrostatic character of the interacting moieties. Ca^{2+} readily binds to proteins, mainly through interaction with sidechains containing deprotonated carboxyl groups, but also through carbonyl and hydroxyl groups with decreasing affinity.[55] Correspondingly, Ca^{2+} has many important biological functions; in particular, there is an important group of lectins ("C-type lectins") which complex carbohydrates in a Ca^{2+}-specific manner.[56] The strongly hydrated Mg^{2+} has been found to form a mixture of inner and outer sphere contacts with both carboxylates and phophates.[55,57,58] Thus, the interaction of divalent cations with carbohydrates containing charged groups may differ from what is seen here with neutral groups.

C. Multiple saccharide-ion interactions

We have investigated structural and dynamical details of alkali cation-saccharide interactions and also the effect of carbohydrate density on these properties. For this purpose, additional simulations were performed on systems mimicking a dense saccharide surface at the same ion concentrations (0.15 M NaCl or KCl). Nine $Man_6GlcNAc_2-Asn$ units were placed in a regular arrangement, each oligosaccharide equally spaced at a distance of approximately 20 Å, with main-chain atoms of the asparagine residues restrained to an imaginary surface, as depicted in Fig. 2. At this distance, the saccharides are close enough to interact with one another, forming a dense carbohydrate layer. This is meant as a zero-order cartoon of a possible situation in the glycocalyx, acknowledging the facts that neither the exact composition of the oligosaccharides in the glycocalyx nor even their distances are known experimentally.

The probability distributions of ion-saccharide coordination numbers for saccharide bound sodium and potassium ions, calculated for the single $Man_6GlcNAc_2$ oligosaccharide (S) and the saccharide array (SA) are shown in Fig. 7. Ion-saccharide coordination numbers are calculated as the number of saccharide oxygens and nitrogens within a distance corresponding to the first minimum of the cation-saccharide distribution functions [Fig. 4(a)]. The maximum numbers of ion-saccharide contacts observed in these simulations are 4 and 7 for Na^+ and K^+, respectively. Although the interaction

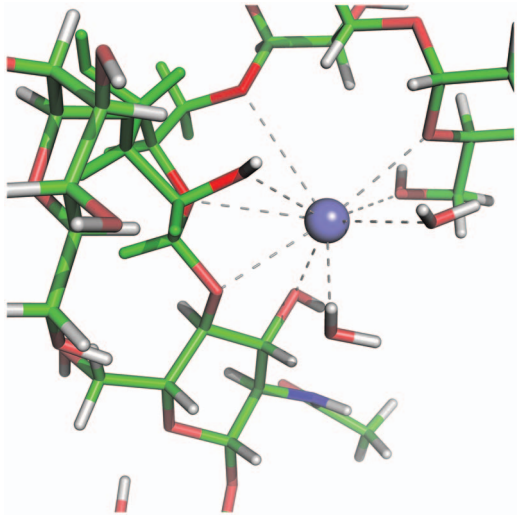

FIG. 8. (Color) A snapshot from the trajectory showing a potassium ion, sevenfold coordinated to the $Man_6GlcNAc_2$ saccharide. Two additional coordinations of the potassium ion to water molecules are also shown. For clarity, the cation is drawn smaller than its usual contact radius. Also, only part of the oligosaccharide is included in this graph, the remainder is cutoff. The figure was generated using PyMOL (Ref. 64).

mainly takes place through a few saccharide contacts for both cations, the larger size and a weaker and more flexible hydration shell of K^+ also allows for higher saccharide coordination numbers, where K^+ is almost fully solvated by the saccharides. A snapshot of the trajectory showing a sevenfold coordinated potassium ion, buried inside an oligosaccharide, can be seen in Fig. 8. The geometrical constraints imposed by Na^+ on the coordinated atoms seem to be hard to meet for the saccharides. Hence, regardless of the saccharide density, no more than fourfold coordinated sodium ions are observed.

Figure 9 shows the layer survival-time-correlation functions $C_R(t)$ defined by Eq. (3). $C_R(t)$ gives the probability that an ion remains within a distance to the closest nonhydrogen saccharide atom, corresponding to the distance of the first minima of the proximal distribution functions in Fig. 4(a), i.e., ions bound to the saccharide, for a time period t. The correlation function can be fitted to a double exponential of the form

$$f(x) = Ae^{(-x/\tau_{\text{short}})} + Be^{(-x/\tau_{\text{long}})}, \tag{5}$$

from which the average residence time can be calculated from the long and short decay constants and the corresponding amplitudes. The decay constants and the calculated average residence times of Na^+ and K^+ are shown in Table II. The

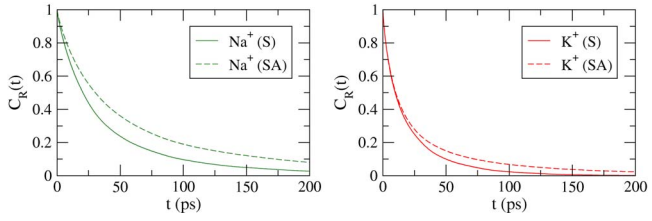

FIG. 9. (Color online) Survival autocorrelation functions for Na^+ (left) and K^+ (right) coordinated to one or more oxygen or nitrogen atoms of $Man_6GlcNAc_2$ (S) (solid lines) or the array of $Man_6GlcNAc_2$ saccharides (SA) (dashed lines).

TABLE II. Temporal characteristics of Na^+ and K^+ interaction with a single $Man_6GlcNAc_2$ saccharide (S) or with an array of $Man_6GlcNAc_2$ saccharides (SA).

	A[a]	τ_{short} [a]	B[a]	τ_{long} [a]	τ_{avg} [b]	n_{scoord} [b]
Na^+(S)	0.62	20.3	0.36	75.6	39.3	1.25
Na^+(SA)	0.55	26.2	0.42	119.3	64.4	1.46
K^+(S)	0.45	7.65	0.50	31.6	19.4	1.32
K^+(SA)	0.64	10.8	0.30	69.8	27.7	1.60

[a]Short and long decay constants τ_{short}, τ_{long} and the corresponding amplitudes A and B of a double exponential [Eq. (5)] fitted to the survival-time-correlation functions in Fig. 9.
[b]τ_{avg} is the average residence time and n_{scoord} is the average cation-saccharide coordination number for saccharide bound ions.

difference in hydration strengths of the two cations is clearly projected onto their interaction with the saccharide. On average, sodium ions can be seen to bind to the saccharide for longer periods of time, in spite of an on average lower saccharide coordination number. The steeper short time decay of the K^+ survival-time-correlation plots in Fig. 9 shows that K^+-saccharide contacts are weaker and have a greater tendency to be broken at shorter time scales, compared to their Na^+ analogs. While the probability for higher coordination numbers increases together with the carbohydrate density, the increase in the residence times for sodium ions is larger. The effect of longer residence times is reflected in the distribution functions and the cumulative sums (not shown here). Thus, although there are on average more potassium ions in the vicinity of the saccharide surface, the relative difference between Na^+ and K^+ is smaller in our saccharide array, compared to the single oligosaccharide simulations. The ion affinities to carbohydrates are therefore expected to depend on the size, shape, and composition of the carbohydrate system and the resulting coordination possibilities.

D. Ion-induced effects on saccharide conformation and flexibility

Many oligosaccharides display a high degree of conformational flexibility and may not have a well-defined three-dimensional shape, but rather exist as an ensemble of conformers in solution at room temperature.[59] The overall conformational flexibility is determined by the flexiblity of the individual glycosidic linkages, joining neighboring sugar residues in the saccharide. The potential energy surface for rotations around the glycosidic linkages can exhibit multiple minima, sometimes separated only by low barriers,[60] allowing for a high conformational flexibility of the whole saccharide on longer time scales, but also conformational rigidity on shorter time scales.[61] *In vacuo*, transitions between different local minima occurs on a time scale of 10–100 ps.[62] In water, transitions occur on much larger time scales, and long simulation times are needed to fully sample the conformational space of an oligosaccharide.[63]

To show the effects ions can impose on saccharide conformation and flexibility, we have taken a closer look at the Man(α1−3)Man glycosidic linkage of the saccharide, connecting residues six and seven in Fig. 1. The average dihedral angles $\langle\phi\rangle$ and $\langle\psi\rangle$ describing this linkage are −40° and

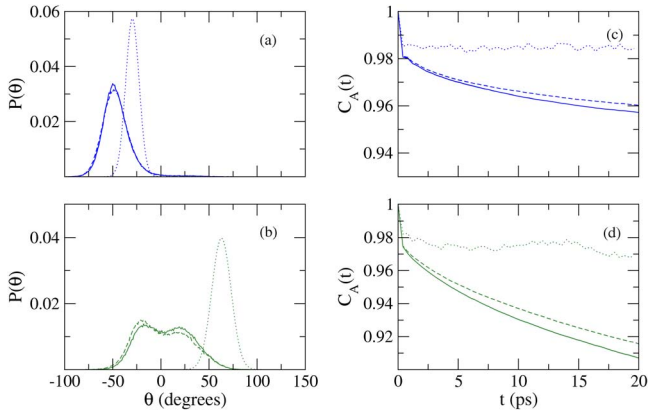

FIG. 10. (Color online) Properties of the two dihedral angles ϕ and ψ describing the Man(α1−3)Man glycosidic linkage connecting residues six and seven of $Man_6GlcNAc_2$. Results from three different trajectories are shown. A full (60 ns) trajectory in water (full lines), the full 0.15 M NaCl trajectory (dashed lines), and a 95 ps long segment of the NaCl trajectory (dotted lines), where a sodium ion is dually bound to oxygens O3 and O6 of residues six and seven. (a) and (b) show the dihedral angle distributions of ϕ and ψ, respectively. For the shorter time segment, the distributions of ϕ and ψ are shown as fitted Gaussian curves. Autocorrelation functions of ϕ and ψ for the different trajectories are shown in (c) and (d).

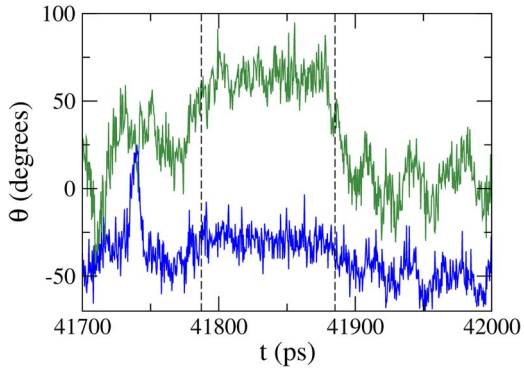

FIG. 11. (Color online) Time histories of the dihedral angles ϕ (lower curve) and ψ (upper curve) describing the Man(α1−3)Man glycosidic linkage connecting residues six and seven of $Man_6GlcNAc_2$ in 0.15 NaCl solution. A time segment where a sodium ion is dually bound to oxygen atoms of residues six and seven is marked with vertical lines.

−15° from nuclear magnetic resonance experiments,[60] but computational studies have shown a considerable flexibility of this linkage due to multiple minima on the conformational energy map.[40,60] Starting with SWEET-derived dihedral angles of −48° and −7.5° for ϕ and ψ, the Man(α1−3)Man configurational space sampled in our trajectories is restricted to the region around the three lowest energy minima (within the lowest-energy superbasin) on the adiabatic Ramachandran energy maps of Naidoo *et al.*[60] Figure 10 shows different properties of the two dihedral angles, ϕ and ψ, for a 95 ps time segment where a sodium ion in dual coordination (to oxygen O6 of residue seven and oxygen O3 of residue six) was observed. As reference, average values from the whole NaCl trajectory, and from a trajectory without any ions, are shown. Figures 10(c) and 10(d) show the dihedral autocorrelation functions calculated from Eq. (4). From these figures, it can be seen that the sodium ion is able to reduce the flexibility of this particular glycosidic linkage and stabilize the saccharide in an intermediate conformation for a short period of time. The dihedral distribution plots in Figs. 10(a) and 10(b) show that the presence of the cation may stabilize the angles in conformations that have low probability to occur when compared to the whole trajectory. For example, for this time segment, the ψ angle is shifted to an average value of 62°, compared to 2° for the whole trajectory. Figure 11 shows the time evolution of the two dihedral angles before, during, and after the interaction with the ion. This figure shows that the conformation of the saccharide clearly is influenced by the cation. During the time the ion is dually bound to the saccharide, in the time interval between 41 790 and 41 885 ps, the ψ angle is shifted toward higher values, allowing the ion to coordinate with oxygens of both carbohydrate residues and relaxes as the ion leaves.

Similar to the ϕ and ψ distributions of the Man(α1−3)Man linkage, the other dihedral angles, determining the total conformation of the saccharide, only show minor differences in water and in the ionic solutions. The only exceptions to this trend are the two 1–6 linkages, which can be seen to populate the three possible staggered conformers, gg, gt, and tg,[23] differently in each simulation. Using a starting structure closest to the gt conformer, the relative populations of the different conformers, for the Man(α1−6)Man glycosidic linkage between residues three and six in Fig. 1, are (100:0:0), (34:63:3), and (81:18:1) in the water, NaCl and KCl simulations, respectively. These differences cannot be attributed to the presence of the ions, but rather show the flexible nature of this particular glycosidic linkage and the long simulation times needed to fully sample the relative populations of the conformers of oligosaccharides.

The dihedral angle correlation plots in Figs. 10(c) and 10(d) show an on average higher short-time correlation for the angles from the NaCl simulation than in pure water. Similar trends can be seen for the other angles, with the general trend that the correlation is higher for the ion-trajectories compared to the pure water simulations, and higher for KCl than for NaCl. Thus, the overall effect of the alkali cations on saccharide conformation is small, but the presence of the ions can induce short time rigidity whenever multiple saccharide coordination occurs.

IV. CONCLUSIONS

We have studied solvation properties of simple cations of biological relevance (focusing on Na^+ and K^+, with additional data on Mg^{2+} and Ca^{2+}), to compare the situation in the bulk with that in a highly complex saccharide environment such as the glycocalyx on eukaryotic cell surfaces. Many features of the glycocalyx, including its density, its composition and also the salt concentration of the surrounding water, vary according to a large number of parameters (cell type, developmental stage, biochemical status, etc.). Nevertheless, we tried to choose a typical setup relatively close to a real glycocalyx situation: The octasaccharide $Man_6GlcNAc_2$ has been taken as a representative glycocalyx unit and the ion concentration was assumed to be 150 mmol in all cases. For investigation of multiple saccharide-ion interactions we have chosen a regular arrangement of nine $Man_6GlcNAc_2$ oligosaccharides, packed as densely as pos-

sible (avoiding aggregation collapse of the oligosaccharides). Therefore, this setup should represent a relevant glycocalyx cut-out, however, it certainly cannot stand for every typical formation of the glycome. We have tested various force field choices and settings, arriving at a combination that is internally consistent and also appears to yield validation results in acceptable agreement with previous theoretical work and with experiment. Hence, we are confident that our results are at least qualitatively correct and possibly extendable to similar glycocalyx oligosaccharides.

Our simulation data for oligosaccharide-cation interactions reveal that K^+ interacts with oligosaccharide oxygen atoms preferentially directly, whereas Na^+ shows an enhanced indirect interaction via an intermediate water molecule (the latter mode is almost exclusively preferred by Mg^{2+} and Ca^{2+}). This agrees with the propensity of Na^+ for holding on more tightly to its first solvation shell water molecules. Accordingly, discounting the indirect water-mediated contacts, there are about twice as many K^+ cations in direct contact with the oligosaccharide, compared to Na^+. The higher flexibility of the first solvation shell of K^+ also allows for up to seven direct cation-oligosaccharide contacts, while Na^+ can have at most four, reflecting the restricted ability of the oligosaccharide to accommodate the more stringent steric preferences around Na^+.

Despite the earlier tendencies favoring oligosaccharide-K^+ contacts, the fewer contacts between the oligosaccharide and Na^+ are longer lived than their K^+ counterparts. Again, this simply reflects the stronger interaction between Na^+ and its first solvation shell: It is harder to induce ligand replacements there, but once it happens, the changed situation is again more stable. In our particular oligosaccharide array setup, these opposed tendencies lead to a decreased difference between Na^+ and K^+ residence times close to the oligosaccharide, when compared to the single oligosaccharide solvation situation.

In general and in detail, these differential solvation effects of saccharides on Na^+ and K^+ differ from what has been found for other biomolecules (proteins, DNA) (with the reservation that charged groups may change this finding). Clearly, this might be important for glycocalyx functions.

Finally, the cations also influence the oligosaccharide conformations. Angular correlations reveal a small but significant overall tendency of Na^+ (and even more so of K^+) to hinder oligosaccharide flexibility. On close inspection of the MD trajectories, the oligosaccharides execute strong but short-lived excursions away from their pure-water preference conformations to temporarily participate in ion solvation.

Our studies might be of high relevance for understanding the biology of the glycocalyx, which is not conclusively recognized until today. It is important to supplement studies on carbohydrate-protein as well as carbohydrate-carbohydrate interactions by the consideration of the role of water and physiological ions and the mechanism of conformational control on cell surfaces. All molecular interactions taken together may finally allow a clue about how the biochemistry of the glycocalyx is orchestrated. In our further studies we will include other relevant oligosaccharide constituents of cell surfaces, including charged molecules such as sialidated glycans or O-sulfated ones such as in the case of HNK-1.

Current work in progress in our laboratories includes oligosaccharide/water simulations with multivalent compounds modeling carbohydrate receptors, as well as free energy simulations of binding between the full bacterial lectin FimH and various mannose mimetics and mannose-containing oligosaccharides, in explicit water including physiological ions.

ACKNOWLEDGMENTS

A generous grant of computer time at the HLRN computing center (Berlin/Hannover) is gratefully acknowledged.

[1] P. Jungwirth and D. J. Tobias, Chem. Rev. **106**, 1259 (2006).
[2] A. Kohlmeyer, C. Hartnig, and E. Spohr, J. Mol. Liq. **78**, 233 (1998).
[3] J. K. Kazimirski and V. Buch, J. Phys. Chem. A **107**, 9762 (2003).
[4] F. Schulz and B. Hartke, Theor. Chem. Acc. **114**, 357 (2005).
[5] C. R. Bertozzi and L. L. Kiessling, Science **291**, 2357 (2001).
[6] J. C. Paulson, O. Blixt, and B. E. Collins, Nat. Chem. Biol. **2**, 238 (2006).
[7] R. A. Dwek, Biochem. Soc. Trans. **23**, 1 (1995).
[8] R. Raman, M. Venkataraman, S. Ramakrishnan, W. Lang, S. Raguram, and R. Sasisekharan, Glycobiology **16**, 82R (2006).
[9] A. Varki, Glycobiology **3**, 97 (1993).
[10] P. H. Seeberger and D. B. Werz, Nature (London) **446**, 1046 (2007).
[11] M. Ambrosi, N. Cameron, and B. Davis, Org. Biomol. Chem. **3**, 1593 (2005).
[12] L. L. Kiessling, J. E. Gestwicki, and L. E. Strong, Angew. Chem. Int. Ed. **45**, 2348 (2006).
[13] J. Rojo, V. Díaz, J. M. de la Fuente, I. Segura, A. G. Barrientos, H. H. Riese, A. Bernad, and S. Penadés, ChemBiolChem. **5**, 291 (2004).
[14] A. Imberty and S. Perez, Chem. Rev. **100**, 4567 (2000).
[15] K. D. Collins, Biophys. J. **72**, 65 (1997).
[16] F. Schulz and B. Hartke, ChemPhysChem **3**, 98 (2002).
[17] S. Bernèche and B. Roux, Nature (London) **414**, 73 (2001).
[18] M. Carrillo-Tripp, H. Saint-Martin, and I. Ortega-Blake, Phys. Rev. Lett. **93**, 168104 (2004).
[19] Y. Cheng, N. Korolev, and L. Nordenskiöld, Nucleic Acids Res. **34**, 686 (2006).
[20] L. Vrbka, J. Vondrásek, B. Jagoda-Cwiklik, R. Vácha, and P. Jungwirth, Proc. Natl. Acad. Sci. U.S.A. **103**, 15440 (2006).
[21] U. Heugen, G. Schwaab, E. Bründermann, M. Heyden, X. Yu, D. M. Leitner, and M. Havenith, Proc. Natl. Acad. Sci. U.S.A. **103**, 12301 (2006).
[22] S. L. Lee, P. G. Debenedetti, and J. R. Errington, J. Chem. Phys. **122**, 204511 (2005).
[23] F. Corzana, M. S. Motawia, C. H. du Penhoat, S. Perez, S. M. Tschampel, R. J. Woods, and S. B. Engelsen, J. Comput. Chem. **25**, 573 (2004).
[24] Q. Liu and J. W. Brady, J. Am. Chem. Soc. **118**, 12276 (1996).
[25] A. Bohne, E. Lang, and C. W. von der Lieth, J. Mol. Model. **4**, 33 (1998).
[26] D. Beglov and J. Roux, J. Chem. Phys. **100**, 9050 (1994).
[27] J. Aaqvist, J. Phys. Chem. **94**, 8021 (1990).
[28] R. J. Woods, C. J. R. A. Dwek, and B. Fraser-Reid, J. Phys. Chem. **99**, 3832 (1995).
[29] W. L. Jorgensen, J. Chandrasekhar, and J. D. Madura, J. Chem. Phys. **79**, 926 (1983).
[30] J. C. Phillips, R. Braun, W. Wang, J. Gumbart, E. Tajkhorshid, E. Villa, C. Chipot, R. D. Skeel, L. Kalé, and K. Schulten, J. Comput. Chem. **26**, 1781 (2005).
[31] H. J. C. Berendsen, J. P. M. Postma, W. F. van Gunsteren, A. DiNola, and J. Haak, J. Chem. Phys. **81**, 3684 (1984).
[32] U. Essmann, L. Parera, M. L. Berkowitz, T. Darden, H. Lee, and L. G. Pedersen, J. Chem. Phys. **103**, 8577 (1995).
[33] J. P. Ryckaert, G. Ciccotti, and H. J. C. Berendsen, J. Comput. Phys. **23**, 327 (1977).
[34] K. N. Kirschner and R. J. Woods, Proc. Natl. Acad. Sci. U.S.A. **98**, 10541 (2001).
[35] D. A. Case, T. A. Darden, T. E. C III, C. L. Simmerling, J. Wang, R. E.

Duke, R. Luo, K. M. Merz, B. Wang, D. A. Pearlman, M. Crowley, S. Bronzell, V. Tsui, H. Gohlke,J. Mongan, V. Hornak, G. Cui, P. Beroza, C. Schafmeister, J. W. Caldwell, W. S. Ross, and P. A. Kollman, AMBER 8, University of California, San Francisco, 2004.
[36] H. S. Ashbaugh, L. R. Pratt, M. E. Paulaitis, J. Clohecy, and T. L. Beck, J. Am. Chem. Soc. **127**, 2808 (2005).
[37] R. W. Impey, P. A. Madden, and I. R. McDonald, J. Phys. Chem. **87**, 5071 (1983).
[38] C. Rocchi, A. R. Bizzarri, and S. Cannistraro, Phys. Rev. E **57**, 3315 (1998).
[39] D. van der Spoel and H. J. C. Berendsen, Biophys. J. **72**, 2032 (1997).
[40] S. W. Homans, Biochemistry **29**, 9110 (1990).
[41] L.-A. Näslund, D. C. Edwards, P. Wernet, U. Bergmann, H. Ogasawara, L. G. M. Petterson, S. Myneni, and A. Nilsson, J. Phys. Chem. A **109**, 5995 (2005).
[42] E. Guardia, D. Laria, and J. Marti, J. Phys. Chem. B **110**, 6332 (2006).
[43] D. Rapaport, *The Art of Molecular Dynamics Simulation*, 2nd ed. (Cambridge Univeristy Press, Cambridge, 2004).
[44] G. Ruocco, M. Sampoli, and R. Vallauri, J. Chem. Phys. **96**, 6167 (1992).
[45] S. Varma and S. B. Rempe, Biophys. Chem. **124**, 192 (2006).
[46] T. Ikeda, M. Boero, and K. Terakura, J. Chem. Phys. **126**, 034501 (2007).
[47] M. Cavallari, C. Cavazzoni, and M. Ferrario, Mol. Phys. **102**, 959 (2004).
[48] D. R. Linde, *CRC Handbook of Chemistry and Physics*, 84th ed. (CRC Press, Boca Raton, 2003).
[49] P. Mark and L. Nilsson, J. Phys. Chem. A **105**, 9954 (2001).
[50] J. E. Enderby and H. H. Electrolyte Monograph, Willis Physics Laboratory, Bristol, UK, 1993.
[51] D. E. Smith and L. X. Dang, J. Chem. Phys. **100**, 3757 (1994).
[52] M. Patra and M. Karttunuen, J. Comput. Chem. **25**, 678 (2004).
[53] J. Wang, P. Cieplack, and P. A. Kollman, J. Comput. Chem. **21**, 1049 (2000).
[54] K. D. Collins, Biophys. Chem. **119**, 271 (2006).
[55] T. Dudev and C. Lim, Chem. Rev. **103**, 773 (2003).
[56] R. B. Dodd and K. Drickamer, Glycobiology **11**, 71R (2001).
[57] A. M. Pyle, J. Biol. Inorg. Chem. **7**, 679 (2002).
[58] M. Egli, Chem. Biol. **9**, 277 (2002).
[59] R. J. Woods, Glycoconj. J. **15**, 209 (1998).
[60] K. J. Naidoo, D. Denysyk, and J. W. Brady, Protein Eng. **10**, 1249 (1997).
[61] C. Höög, C. Landersjö, and G. Widmalm, Chem. Eur. J. **7**, 3069 (2001).
[62] J. P. Carver, Pure Appl. Chem. **65**, 763 (1993).
[63] C. S. Pereira, D. Kony, R. Baron, M. Müller, W. F. van Gunsteren, and P. H. Hünenberger, Biophys. J. **90**, 4337 (2006).
[64] W. DeLano, DeLano Scientific, Palo Alto, CA, 2002.